Reference: Spearpoint M J, Quintiere J G. Predicting the ignition of wood in the Cone Calorimeter - effect of species, grain orientation and heat flux. Fire Safety Journal, Vol 36/4, pp. 391-415, 2001.

PREDICTING THE PILOTED IGNITION OF WOOD IN THE CONE CALORIMETER USING AN INTEGRAL MODEL - EFFECT OF SPECIES, GRAIN ORIENTATION AND HEAT FLUX

M. J. Spearpoint and J. G. Quintiere
Department of Fire Protection Engineering
University of Maryland

ABSTRACT

This paper experimentally and theoretically examines the ignition of 50 mm thick samples of wood in the Cone Calorimeter. Four species of wood were exposed to a range of incident heat fluxes up to 75 kW/m^2 with their grain oriented either parallel or perpendicular to the incident heat flux. The time to ignition measurements obtained from the Cone Calorimeter were used to derive characteristic properties of the materials. These properties were used as input to a one-dimensional integral model that describes the transient pyrolysis of a semi-infinite charring solid subject to a constant radiant heat flux.

The integral model predictions and experimental data compare well at incident heat fluxes above around 20 kW/m^2. At lower heat fluxes it was found that the ignition mechanism of wood is different from that at higher incident fluxes. This difference is believed to be due to char oxidation that precedes flaming ignition.

The lowest radiant heat flux to cause ignition was found to be approximately 10 kW/m^2 depending on species, grain orientation or moisture content. Ignition at low heat fluxes could take up to 1½ hours.

NOMENCLATURE

α	thermal diffusivity, [m^2/s], absorptivity [-]
A	area, [m^2]
β	ratio of convective gain and radiative loss with incident heat flux, [-]
c	specific heat, [J/kg.K]
C	ignition constant, [-]
δ	depth, [m]
f	grain orientation coefficient, [-]
η	height, [m]
h	heat transfer coefficient [$W/m^2.K$]
I	thermal inertia, $k\rho c$, [$J^2.m^{-4}.K^{-2}.s^{-1}$]
k	thermal conductivity, [W/m.K]
m	mass, [kg]
q	heat flux, [W/m^2]
ρ	density, [kg/m^3]
s	specific gravity, [-]
T	temperature, [°C] or [K]
t	time, [s]
τ	dimensionless time, [-]
σ	Stefan-Boltzmann constant [$W/m^2.K$]
Z	constant used in pure convective loss ignition analysis, [-]

Subscripts

0	initial, ambient
c	convective
cr	critical
f	final
i	incident
ig	ignition
p	pyrolysis
s	surface
v	vaporisation
w	virgin wood

Superscripts

$( )''$	per unit area
$(\dot{})$	per unit time

1. INTRODUCTION

Ever since prehistoric times humans have known that wood burns and the ability of wood to burn has been both a benefit and a problem. The capability to predict the burning rate of wood in modern times has become increasingly important as fire safety engineering moves toward a performance-based approach to building design. For example, computer based fire and hazard models require the burning rate of materials to be specified as input.

The pyrolysis behaviour of solid materials can be divided into two types: non-charring and charring. Non-charring materials burn away completely leaving no residue and can be modelled using theory similar to flammable liquids. In contrast, charring materials leave relatively significant amounts of residue when they burn. The pyrolysis of charring materials such as wood is a complex interplay of chemistry, heat and mass transfer. Charring materials must be modelled in terms of a pyrolysis front penetrating into the material with an increasing surface temperature and without a well-defined steady state.

The purpose of this paper is to examine the ignition behaviour of wood and compare those results to a one-dimensional integral model for charring materials. The experimental data used in this paper is taken from the work by Spearpoint [1] in which the ignition and burning rate of several species of wood were measured in the Cone Calorimeter [2]. The analysis of the burning rate data and comparison with the theory is to be published elsewhere [3].

2. PREVIOUS STUDIES

2.1 General

There is a substantial volume of work in the literature regarding the ignition, pyrolysis, burning and charring behaviour of wood (and cellulosic materials). It is not the intent of this work to reference and review every study conducted, but a brief summary will be presented.

Kanury [4] gives a general overview of the ignition of solids by thermal radiation or convection. Roberts [5] reviewed the role of kinetics for the pyrolysis of wood and

related materials. Simms [6] examined the role of thermal radiation on the damage to cellulosic solids by considering the chemical and thermal histories of the material. Work on char rate in wood includes studies by Kanury [7] who examined the phenomenon using Arrhenius pyrolysis kinetics. A detailed study of the pyrolysis kinetics of cellulose has been conducted by Suuberg, Milosavljevic & Lilly [8].

Atreya and co-workers have done extensive work on the ignition and burning of wood. In his initial work Atreya [9] included experimental observations for the piloted ignition of wood and identified several important factors. Later these were incorporated in a detailed finite difference ignition model developed by Tzeng & Atreya [10]. Abu-Zaid & Atreya [11] considered the effect of moisture on the ignition of cellulosic materials. Further work by Atreya, Carpentier & Harkleroad [12] examined the effect of sample orientation on piloted ignition and flame spread on wood.

2.2 Ignition and burning rate models

Several models for the burning rate of solid materials, both charring and non-charring, have been developed. Examples include the studies by Delichatsios & de Ris [13]; Chen *et al.* [14]; Wichman & Atreya [15]; Yuen *et al.* [16] and Parker [17]. These models range from simple treatments of the ignition and burning process using pure heat conduction models to the use of complex chemical kinetics for the pyrolysis of a charring material. Many of the models consist of complex computational codes that require a relatively large number of property values to complete their predictions. These many factors can (at least at present) limit the use of such models since many of the properties are difficult to practically obtain and the codes may not be suitable for incorporation into more general fire hazard models.

In this paper, we examine the integral model initially developed by Quintiere [18]. A one-dimensional pyrolysis model which includes the processes of charring, vaporisation, flame and heat conduction effects was proposed. This model was further developed by Quintiere & Iqbal [19] to solve the one-dimensional unsteady heat transfer equations during the pre-heating and gasification periods using an integral method. Anderson [20] studied the integral solution to the model and compared the integral solution with the exact solution. Finally, in the study conducted by Hopkins

[21], the model was compared against experimental data for non-charring thermoplastics tested in the Cone Calorimeter.

A nearly identical integral model for the burning of a charring material was also successfully demonstrated by Moghtaderi, Novozhilov, Fletcher & Kent [22] by validation with an exact numerical solution and with experimental data.

2.3 Experimental data

Janssens [23], [24], [25] tested several species of wood in the Cone Calorimeter with the samples tested in the vertical orientation and the grain perpendicular to the incident heat flux (i.e. equivalent to the *along* grain orientation defined in this paper). The burning characteristics of wood have been measured by Tran & White [26] using the Ohio State University (OSU) apparatus at a range of incident heat fluxes between around 17 and 56 kW/m^2.

Other experimental data have been reported by Parker [27] for Douglas fir and Dietenberger [28] for Redwood in both the LIFT and Cone Calorimeter. The study by Hopkins [21] also includes data for two charring materials, namely Redwood and Red Oak, but no detailed analysis or comparison with the integral model was conducted with these data.

3. EXPERIMENTAL TEST PROGRAM

3.1 General

The wood samples were provided such that the grain was parallel to the incident heat flux (i.e. cut *across* the grain) and perpendicular to the incident heat flux (i.e. cut *along* the grain) as shown in Figure 1. Four species of wood were tested in the study: Douglas fir, Redwood, Red oak and Maple. Douglas fir and Redwood are both softwoods whereas Red oak and Maple are both hardwoods. The samples were all cut from the sapwood portion of sections of lumber and were nominally 50 mm thick by 96 mm square.

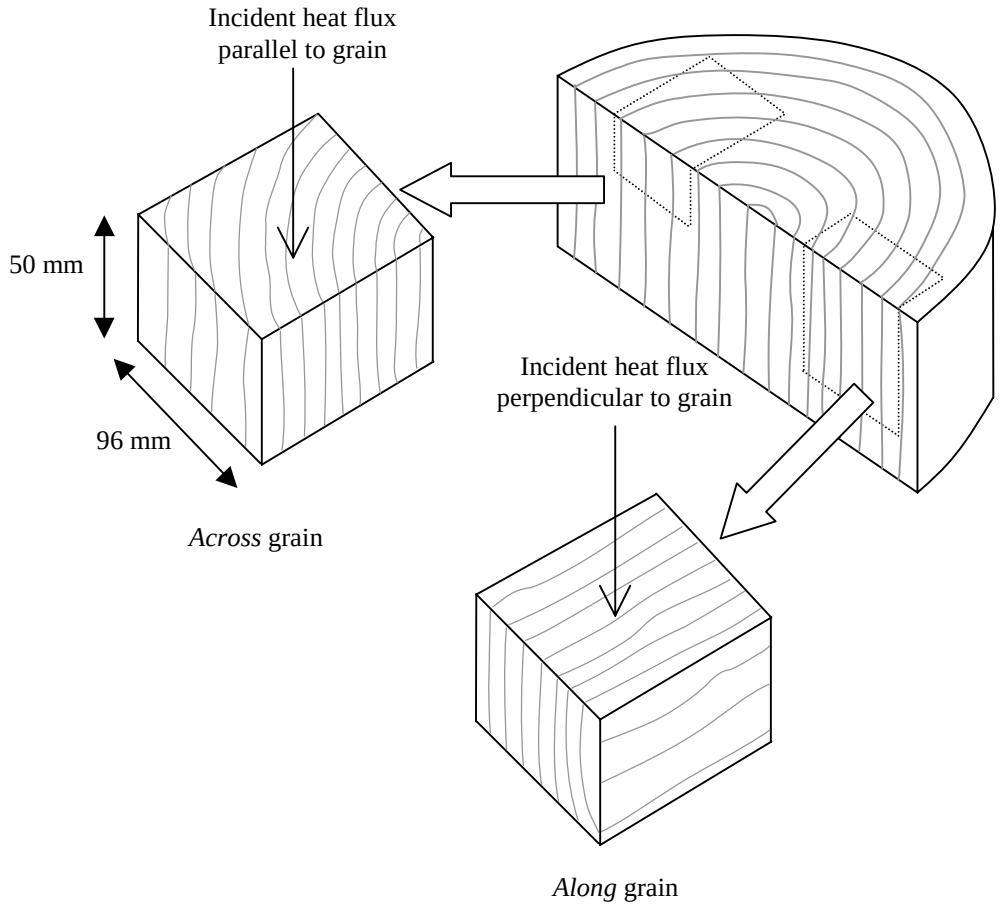

Figure 1. Sample grain configurations.

Samples were stored in a desiccator at nominally 50 % relative humidity and 20 °C. The moisture content of each sample was measured with a hand-held moisture meter prior to exposure (Table 2) within the limits of the instrument. All samples were tested in the Cone Calorimeter in the horizontal orientation. Samples were wrapped in a single layer of aluminium foil, placed into the sample holder and backed by low density ceramic fibre insulation material. In most tests the layer of ceramic fibre blanket was necessarily thin since the maximum height of the sample retainer frame is 50 mm. The doors to the combustion chamber were closed during the experiments and air was provided by a vent in the base of the chamber below the load cell. Sustained ignition is defined as when the sample continues to flame for an uninterrupted period of at least 10 s.

3.2 Burning rate tests

The main 'burning rate' series of 54 tests were conducted at the University of Maryland by the authors on behalf of Schroeder [29] as part of his analysis of the change in the structure of materials when exposed to an external heat flux for relatively prolonged durations. The tests included the measurement of time to ignition, mass loss, rate of heat release and smoke extinction data. Incident heat fluxes of 25 kW/m^2, 35 kW/m^2, 50 kW/m^2 and 75 kW/m^2 were selected for these experiments. For the majority of the burning rate tests, exposure times of 25 minutes were used, however, in a few cases the exposure time was extended to 75 minutes.

3.3 Ignition tests

A total of 41 'ignition only' tests at lower heat fluxes were conducted where only time to ignition was measured. These tests were conducted between heat fluxes below 25 kW/m^2 down to heat fluxes in the region of the critical heat flux for ignition for a particular species of wood at a particular grain orientation. The critical heat flux is defined as the minimum external heat flux required to achieve piloted ignition of an exposed sample. In these 'ignition only' tests, the sample was exposed to the external heat flux until sustained flaming ignition occurred or until it was determined by observation that ignition was unlikely to take place. If ignition occurred, the sample was extinguished immediately.

The selection of a 'failure to ignite' criterion is somewhat subject to operator interpretation and patience. The ASTM standard for the Cone Calorimeter [2] suggests in paragraph 11.2.8

> *If the specimen does not ignite in 10min, remove and discard, unless the specimen is showing signs of heat evolution.*

Similarly, the ASTM standard for the Lateral Ignition and Flame Test (LIFT) apparatus [30] suggests in its paragraph 11.2.8

> *The test is considered complete if ignition does not occur within 20 min. However, this is an arbitrary cut-off, and longer times can be considered.*

Clearly both of these test methods leave the ultimate decision as to when ignition has not (or will not occur) to the operator and the requirements of the particular

experiment. In this study the decision as to when to terminate a test was of particular importance in determining the critical heat flux for ignition.

In the 'ignition only' tests single 50 mm thick samples of wood were cut into four equal thickness slices. For each test, the four slices were stacked in the sample holder to mimic the full thickness samples used in the main test series. Critical heat flux measurements were not conducted for Red oak since all samples were used in the main 'burning rate' experiments.

Prior to ignition it was noted that some samples would warp either away from or towards the cone heater. The warping was seen to 'self-correct' (i.e. return to almost level) in some instances. In addition, coupled with shrinkage, there were cases of the sample warping slightly out of the retainer frame at one corner or along an edge. These factors may have introduced some variation into the ignition results since the sample may have ignited sooner or later than if it had remained uniformly level.

In the tests conducted in this study it was found that the wood continued to ignite even at very low incident heat fluxes i.e. below 10 kW/m^2, which is considerably lower than values quoted in the literature. It was observed that at these low heat fluxes, a localised glowing could be seen on the surface of the wood prior to ignition. In such cases, flaming ignition would eventually occur with the flames initially limited to the region of glowing but gradually spreading over the exposed surface of the sample. In contrast, at higher heat fluxes the sample would immediately ignite over the complete surface of the sample. It is likely that this localised glowing contributed an additional source of energy to that provided by the heater to the surface of the wood eventually leading to ignition. This low heat flux domain might be considered to possess two ignitions (1) glowing and (2) flaming.

Martin [31] alludes to this change in the ignition mechanism at low heat fluxes. He suggests that the ignition behaviour of cellulose can be split into three regions; convection-controlled, diffusion-controlled and ablation-controlled. We interpret Martin as (1) convection controlled (very low flux): ignition time controlled by diffusion of oxygen into vaporised fuel and hot surface; (2) diffusion-controlled: the ignition time is controlled by thermal (diffusion) conduction, as in our integral model;

(3) ablation-controlled (very high flux): ignition time controlled by the time to vaporise the surface fuel. He further notes that cellulose exhibits basically two kinds of ignition phenomena without the presence of a pilot flame - spontaneous flaming and glowing ignition.

4. THERMO-PHYSICAL MATERIAL PROPERTIES

The integral model requires a number of properties to be obtained for the material. A few of the properties can be easily measured, others can be obtained from experimental data and the remainder may be obtained from the literature.

The determination of fundamental material properties can be a complex process. For the pyrolysis of wood we require the thermal conductivity k, density ρ and specific heat c and the related properties of thermal inertia $I = k\rho c$ and thermal diffusivity $\alpha = k/\rho c$. These properties may vary as the material undergoes thermal, mechanical and chemical changes.

4.1 Density

The density of wood is primarily dependent on the species but it will also vary by individual tree and within that individual tree. Any moisture in the wood will also affect the density. In this study, the average bulk density of each sample was calculated from its mass and volume such that

$$\rho_w = \frac{m_{w,0}}{A_0.\eta_{w,0}}, \tag{1}$$

where A_0 is the surface area of the exposed face of the sample and $\eta_{w,0}$ is the initial height of the sample. In this study, the mass and dimensions were recorded prior to testing and the density simply obtained from Equation (1).

4.2 Moisture content

The moisture content of wood may be assumed to be a pseudo-property of the material and, as described in Section 4.3 and Section 4.4, it can have an influence on the thermal conductivity and specific heat and thus the ignition characteristics of wood. The moisture content is a function of the species of wood and the conditions in

which it is stored. The study by the Fire Officers Committee quoted by Cholin [32] demonstrates how the increase in the moisture content of wood increases the time to ignition for a given incident heat flux.

4.3 Thermal conductivity

The study by Fredlund [33] describes how the thermal conductivity varies in wood with emittance, density, moisture content, temperature and the type of gas enclosed in the material. Thermal conductivity increases markedly with increasing moisture content, being about twice as high at 100 per cent moisture content as it is at 10 per cent.

The thermal conductivity also depends on the orientation of the grain of the wood. According to the Wood Engineering Handbook [34], the thermal conductivity of wood is approximately 2.0 to 2.8 greater along the grain than perpendicular to the grain. Fredlund [33] quotes a study that gives the range of ratios as between 1.75 and 2.25. Desch & Dinwoodie [35] quote values for the thermal conductivity of Spruce and European oak for the various grain orientations (parallel or tangential/radial). The ratios of the values give 2.10 and 1.75 for Spruce and European oak respectively. From these literature data it is assumed in this paper that the increase in the thermal conductivity for the samples tested *across* the grain is typically 2.1 times greater than *along* the grain for any species of wood.

4.4 Specific heat

The specific heat of wood increases with temperature but is practically independent of density or species. For oven-dry wood, Desch & Dinwoodie [35] give the specific heat as 1,360 J/kg.K. When wood contains water, the specific heat is greater than dry wood because of the larger specific heat of water. The apparent specific heat of moist wood is larger than the simple sum of the separate effects of wood and the water. This is due to the thermal energy absorbed by the wood-water bonds.

4.5 Thermal inertia and thermal diffusivity

Since the thermal inertia and the specific heat of wood are temperature dependent, the thermal inertia at ignition is not that obtained at ambient conditions. Instead the

thermal inertia at ignition is an 'apparent' value and it will be shown in § 6.2 that this apparent thermal inertia can be obtained from ignition data.

In the study by Parker [27] it was shown that the thermal diffusivity of Douglas fir remained at an almost constant value of 2.1 x 10^{-7} m^2/s up to temperatures of approximately 250 °C. Similarly, Suuberg *et al.* [8] found that the thermal diffusivity of raw cellulose remained constant at 0.86 x 10^{-7} m^2/s ±22% between 116 °C and 289 °C. Janssens [36] also quotes work in which it is suggested that the thermal diffusivity is independent of temperature. Thus it is assumed that the thermal diffusivity is constant for each given species of wood.

The values of the thermal diffusivities perpendicular to the grain used in this study are given in Table 1. The value for Douglas Fir is taken from Parker [27] and the value for Redwood taken from Dietenberger [28]. Values for Maple and Red Oak were not found in the literature and so these had to be estimated by simply taking the average of the two known values quoted.

Species	Thermal diffusivity $[m^2/s]$
Redwood	1.65 x 10^{-7}
Red Oak	1.88 x 10^{-7}
Douglas Fir	2.10 x 10^{-7}
Maple	1.88 x 10^{-7}

Table 1. Thermal diffusivity values for species of wood tested.

Taking an average value was justified by the fact that, according to the Wood Engineering Handbook [34], the typical value for the thermal diffusivity of wood is 1.61 x 10^{-7} m^2/s and this value decreases with specific gravity *s* over the range of 0.30 to 0.65 by 0.65 x 10^{-7} m^2/s where the specific gravity of wood is based on its weight when oven dry and volume at 6% moisture content.

Assuming that the typical value for the thermal diffusivity is at the mid-range of the specific gravity (i.e. for a specific gravity of 0.48), the variation of thermal diffusivity

with specific gravity can be compared with the values quoted by Parker [27] and Dietenberger [28] (Figure 2) using the specific gravity values for the two species [34].

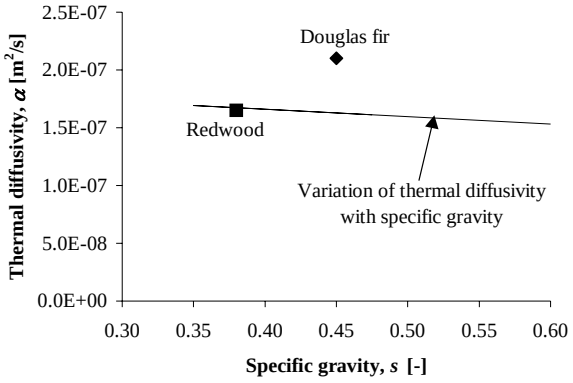

Figure 2. Variation of thermal diffusivity with specific gravity.

The data quoted by Parker and Dientenberger closely match the relationship given in the Wood Engineering Handbook. Furthermore, there is almost negligible change in the thermal diffusivity over the specified range of specific gravities. Thus, the estimated values for the thermal diffusivity for Maple and Red oak appear reasonable.

Using the definitions for the thermal inertia and diffusivity, apparent values for the thermal conductivity and the specific heat can be obtained. However, as discussed in Section 4.3, the thermal conductivity of wood increases by a factor of around 2.1 along the grain compared to perpendicular to the grain. Hence a factor *f* of 2.1 is introduced for the *across* grain orientation thermal diffusivity. Thus,

$$f\alpha = \frac{k}{I/k} \tag{2}$$

where f = 1 for the *along* grain samples and f = 2.1 for the *across* grain orientation. Rearranging to solve for k we get

$$k = \sqrt{f\,\alpha\, I} \tag{3}$$

and we can find c from

$$c = \frac{I}{k\rho}\,. \tag{4}$$

4.6 Emissivity

In this study the emissivity of the surface of the wood is assumed to be unity. Janssens [23] quotes several sources regarding the emissivity and absorptivity of wood that suggest the absorptivity of virgin wood is on average 0.76, independent of species. After thermal exposure begins, this value changes due to the darkening of the surface as it chars. The emissivity of oven dry wood varies between 0.60 and 0.72 depending on species. Finally, the assumption that Kirchoff's law ($\alpha = \varepsilon$) holds is reasonable for most analyses. Thus we might expect the emissivity to be around 0.72 prior to exposure and this value to approach 1 as the surface chars due to the external heat flux.

5. THEORY

5.1 The integral model

The integral analysis for ignition was developed by Quintiere [18] assuming ignition based on a critical temperature of the surface due to an applied radiative heat flux.

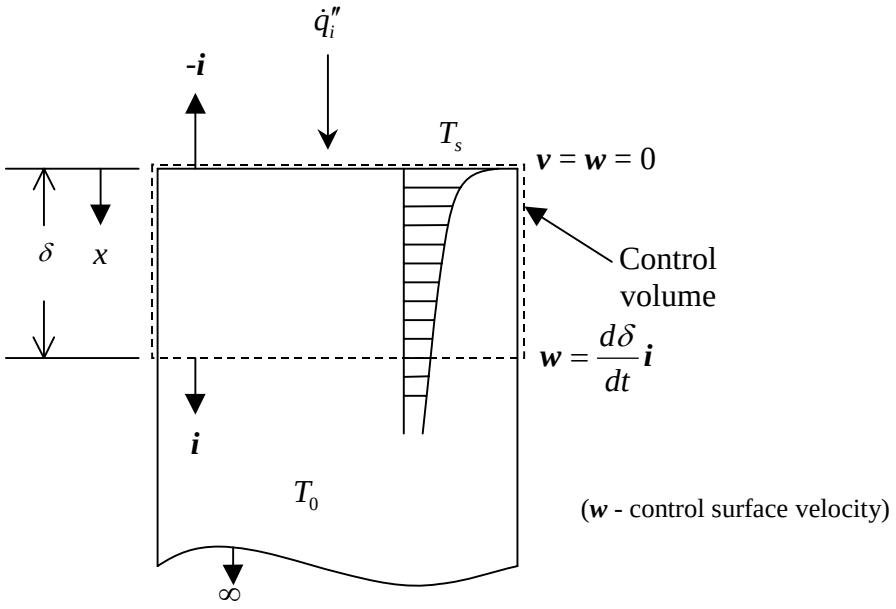

Figure 3. Integral model ignition scenario.

The following assumptions are made for the ignition model:

(a) Ignition occurs when the surface temperature achieves a critical value, T_{ig}

(b) Solid is inert up to ignition and

(c) Solid is infinitely thick

The thermal heating of the solid is depicted by a thermal penetration layer of depth $\delta(t)$ as shown in Figure 3. By considering the incident heat flux and the losses due to radiation and convection, the net heat flux at a given time t is given by

$$\dot{q}''(t) = \alpha \dot{q}_i'' - \varepsilon \sigma (T_s^4 - T_0^4) - h_c (T_s - T_0) \tag{5}$$

where the emissivity ε and the absorptivity α are assumed to be 1 as discussed in § 4.6, thus $\dot{q}''(t)$ becomes

$$\dot{q}''(t) = \dot{q}_i'' - \sigma (T_s^4 - T_0^4) - h_c (T_s - T_0) . \tag{6}$$

Conservation of energy for the control volume obtains

$$\rho c \left[\frac{d}{dt} \int_0^{\delta} T(x) dx - T_0 \frac{d\delta}{dt} \right] = \dot{q}''(t) \tag{7}$$

where c is the specific capacity of the wood at a mean temperature up to T_{ig} and ρ is the density of wood $\rho \equiv \rho_w$ since we assume the density remains constant. Since

$$\frac{d}{dt} \int_0^{\delta} (T - T_0) dx = \frac{d}{dt} \int_0^{\delta} T \, dx - T_0 \frac{d\delta}{dt} . \tag{8}$$

Then, from Equation (7) and Equation (8)

$$\rho c \frac{d}{dt} \int_0^{\delta} (T - T_0) dx = \dot{q}''(t) . \tag{9}$$

The following temperature profile is selected through the region δ

$$T - T_0 = \frac{\dot{q}''(t)\delta}{2k} \left(1 - \frac{x}{\delta} \right)^2 \tag{10}$$

such that the boundary conditions are

$$\text{(i)} \qquad \text{when } x = 0, \quad \dot{q}''(t) = -k \frac{\partial T}{\partial x} \tag{11}$$

$$\text{(ii)} \qquad \text{when } x = \delta, \quad T = T_0 \tag{12}$$

$$\text{(iii)} \qquad \text{when } x = \delta, \quad k \frac{\partial T}{\partial x} = 0 \qquad i.e. \text{no heat loss} \tag{13}$$

where k is the thermal conductivity of the wood at ignition.

Substituting Equation (10) into Equation (9) gives

$$\frac{d}{dt}\dot{q}''(t)\delta^2 = 6\frac{k}{\rho c}\dot{q}''(t) \tag{14}$$

and thus by integrating

$$\dot{q}''\delta^2 = 6\frac{k}{\rho c}\int_0^t \dot{q}''(t)\,dt\,. \tag{15}$$

If we assume that the net heat flux is the average of the heat flux at time = 0, i.e. $\dot{q}''(0)$ and at time = t, i.e. $\dot{q}''(t)$ then

$$\int_0^t \dot{q}''(t)\,dt = \left[\frac{\dot{q}''(t)+\dot{q}''(0)}{2}\right]t \tag{16}$$

thus substituting Equation (16) into Equation (15)

$$\dot{q}''(t)\delta^2 = 6\frac{k}{\rho c}\left[\frac{\dot{q}''(t)+\dot{q}''(0)}{2}\right]t\,. \tag{17}$$

From Equation (6), at time $t = 0$, the surface temperature is at ambient i.e. $T_s = T_0$ thus

$$\dot{q}''(0) = \dot{q}_i'' \tag{18}$$

and at time $t = t_{ig}$, we assume that the surface temperature is at the ignition temperature, $T_s = T_{ig}$ thus

$$\dot{q}''(t_{ig}) = \dot{q}_i'' - \sigma(T_{ig}^4 - T_0^4) - h_c(T_{ig} - T_0) \tag{19}$$

Equation (6), can be expressed as

$$\frac{\dot{q}''(t)}{\dot{q}_i''} = 1 - \frac{\sigma(T_s^4 - T_0^4) + h_c(T_s - T_0)}{\dot{q}_i''} \tag{20}$$

Let

$$\beta \equiv \frac{\sigma(T_s^4 - T_0^4) + h_c(T_s - T_0)}{\dot{q}_i''} \tag{21}$$

$$\therefore \qquad \dot{q}''(t) = \dot{q}_i''(1-\beta). \tag{22}$$

The parameter β characterises the magnitude of radiation and convective losses relative to the incident heat flux. Substituting Equation (18) and Equation (22) into Equation (17) we obtain

$$\delta^2 = 3\frac{k}{\rho c}\left[\frac{2-\beta}{1-\beta}\right]t\,. \tag{23}$$

If we consider the surface at the time of ignition and assume that the surface temperature is at the ignition temperature $t = t_{ig}$, $T_s = T_{ig}$, $x = 0$, then from Equation (10)

$$\left(T_{ig} - T_0\right)^2 = \frac{\left[\dot{q}''\left(t_{ig}\right)\right]^2 \delta^2}{4k^2}. \tag{24}$$

Substituting Equation (23) into Equation (24)

$$t_{ig} = \frac{4}{3} k\rho c \left[\frac{1-\beta_{ig}}{2-\beta_{ig}}\right] \frac{\left(T_{ig} - T_0\right)^2}{\left[\dot{q}''\left(t_{ig}\right)\right]^2} \tag{25}$$

where from Equation (22)

$$\dot{q}''\left(t_{ig}\right) = \dot{q}_i''\left(1-\beta_{ig}\right) \tag{26}$$

and from Equation (21)

$$\beta_{ig} \equiv \frac{\sigma(T_{ig}^4 - T_0^4) + h_c(T_{ig} - T_0)}{\dot{q}_i''}. \tag{27}$$

When $\dot{q}_i''$ is large, from Equation (21), $\beta_{ig} \to 0$, thus from Equation (25)

$$t_{ig} \approx \frac{2}{3} k\rho c \frac{\left(T_{ig} - T_0\right)^2}{\left(\dot{q}_i''\right)^2}. \tag{28}$$

The 2/3 coefficient has been found to be $\pi/4$ in the more exact (pure convective loss) solution of this problem (see Section 5.2). Substituting Equation (26) into Equation (25) we obtain

$$t_{ig} = \frac{4}{3} k\rho c \left[\frac{1}{\left(2-\beta_{ig}\right)\left(1-\beta_{ig}\right)}\right] \frac{\left(T_{ig} - T_0\right)^2}{\dot{q}_i''^2}. \tag{29}$$

Or alternatively

$$t_{ig} = C_{ig} k\rho c \frac{\left(T_{ig} - T_0\right)^2}{\dot{q}_i''^2} \tag{30}$$

where

$$C_{ig} = \frac{4}{3}\left[\frac{1}{\left(2-\beta_{ig}\right)\left(1-\beta_{ig}\right)}\right]. \tag{31}$$

As $\beta_{ig} \to 1$, Equation (31) approaches ∞ and thus from Equation (30), $t_{ig} \to \infty$ also. As the time to ignition increases we are approaching the critical heat flux for ignition. From Equation (27) with $\beta_{ig} \to 1$

$$1 \approx \frac{\sigma(T_{ig}^4 - T_0^4) + h_c(T_{ig} - T_0)}{\dot{q}_i''} \tag{32}$$

or alternatively, with $\dot{q}_{cr}'' \equiv \dot{q}_i''$ as $t \to \infty$

$$\dot{q}_{cr}'' = \sigma(T_{ig}^4 - T_0^4) + h_c(T_{ig} - T_0)\,. \tag{33}$$

Thus from Equation (27)

$$\beta_{ig} \equiv \frac{\dot{q}_{cr}''}{\dot{q}_i''}\,. \tag{34}$$

5.2 Comparison of approximate solutions for ignition

The approximate solution for ignition from the integral model can be compared with the exact solution for convective heat loss only and the approximate solutions by Delichatsios, Panagiotou & Kiley [37].

a) For the exact solution for convective heat loss only, Drysdale [38] states that

$$\frac{T - T_0}{T_\infty - T_0} = 1 - \exp\left(\frac{\alpha t}{(k/h_c)^2}\right).\mathrm{erfc}\left(\frac{\sqrt{\alpha t}}{k/h_c}\right). \tag{35}$$

Given, from Equation (6), for convection only

$$\dot{q}_i'' = h_c\left(T_\infty - T_0\right)$$

thus Equation (35) can expressed as

$$\frac{T_{ig} - T_0}{\left(\dot{q}_i''/h_c\right)} = 1 - e^{\gamma^2}\,\mathrm{erfc}(\gamma) \tag{36}$$

where

$$\gamma \equiv h_c\sqrt{\frac{t_{ig}}{k\rho c}}\,. \tag{37}$$

From Carslaw & Jaeger [38], when $\gamma \to \infty$

$$\frac{\sqrt{\pi}}{2}\mathrm{erfc}(\gamma) \approx \frac{e^{-\gamma^2}}{2\gamma} \tag{38}$$

or rearranging Equation (38)

$$\operatorname{erfc}(\gamma) \approx \frac{e^{-\gamma^2}}{\sqrt{\pi}\gamma}. \tag{39}$$

Then, from Equation (36) and Equation (39)

$$\lim_{\gamma\to\infty}\left(1 - e^{\gamma^2}\operatorname{erfc}(\gamma)\right) = 1 - \frac{1}{\sqrt{\pi}\gamma} \to 1. \tag{40}$$

From Equation (33), neglecting radiation heat losses, as $t_{ig} \to \infty$

$$\dot{q}_i'' = h_c(T_{ig} - T_0) \equiv \dot{q}_{cr}''. \tag{41}$$

When $t_{ig} \to 0$ or $\gamma \to 0$, from Carslaw & Jaeger [38],

$$\operatorname{erf}(\gamma) \approx \frac{2}{\sqrt{\pi}}\gamma. \tag{42}$$

By expansion of the right-hand side of Equation (36)

$$1 - e^{\gamma^2}\operatorname{erfc}(\gamma) \approx 1 - \left(1 + \gamma^2 + ...\right)\left(1 - \frac{2}{\sqrt{\pi}}\gamma + ...\right)$$

$$\approx 1 - 1 + \frac{2}{\sqrt{\pi}}\gamma = \frac{2}{\sqrt{\pi}}\gamma. \tag{43}$$

Thus substituting Equation (43) and Equation (37) into Equation (36) the time to ignition is

$$t_{ig} = \frac{\pi}{4}k\rho c\left(\frac{T_{ig} - T_0}{\dot{q}_i''}\right)^2. \tag{44}$$

To make the approximate integral solution given in Equation (29) fit the limit of the exact (pure convective loss) solution, let

$$\frac{Z}{\left(2 - \beta_{ig}\right)\left(1 - \beta_{ig}\right)} = \frac{\pi}{4} \tag{45}$$

where Z is a new constant in place of the 4/3 given in Equation (29). At high incident heat fluxes, $t_{ig} \to 0$ and $\beta_{ig} \to 0$, thus

$$\frac{Z}{2} = \frac{\pi}{4} \qquad \text{or} \qquad Z = \frac{\pi}{2}$$

therefore, substituting for Z the 4/3 in Equation (29) we obtain

$$t_{ig} = \frac{\pi}{2}k\rho c\left[\frac{1}{\left(2 - \beta_{ig}\right)\left(1 - \beta_{ig}\right)}\right]\frac{\left(T_{ig} - T_0\right)^2}{\dot{q}_i''^2} \tag{46}$$

or

$$\frac{1}{\sqrt{t_{ig}}} = \frac{1}{\sqrt{\pi k\rho c}} \sqrt{2\left(2-\beta_{ig}\right)\left(1-\beta_{ig}\right)} \frac{\dot{q}_i''}{\left(T_{ig}-T_0\right)}. \tag{47}$$

b) In the study by Delichatsios, Panagiotou & Kiley [37], the authors suggest that when the incident heat flux is greater than about three times the critical heat flux (i.e. $\dot{q}_i'' > 3\dot{q}_{cr}''$) then

$$\frac{1}{\sqrt{t_{ig}}} = \frac{2}{\sqrt{\pi k\rho c}} \frac{1}{\left(T_p - T_0\right)} \left[\dot{q}_i'' - 0.64\dot{q}_{cr}''\right] \tag{48}$$

and when the incident heat flux is less than 1.1 times the critical heat flux (i.e. $\dot{q}_i'' < 1.1\dot{q}_{cr}''$) then

$$\frac{1}{\sqrt{t_{ig}}} = \frac{\pi}{\sqrt{\pi k\rho c}} \frac{\dot{q}_i'' - \dot{q}_{cr}''}{\left(T_p - T_0\right)} \tag{49}$$

where T_p is the pyrolysis temperature and the critical heat flux ignores convective heat fluxes which are considered by Delichatsios *et al.* to be negligible, that is

$$\dot{q}_{cr}'' = \sigma(T_{ig}^4 - T_0^4). \tag{50}$$

Defining the following dimensionless heat flux and time variables as

$$\frac{1}{\beta_{ig}} \equiv \frac{\dot{q}_i''}{\dot{q}_{cr}''} \tag{51}$$

and

$$\tau_{ig} \equiv \frac{\dot{q}_{cr}''^{\,2} t_{ig}}{\left(T_{ig} - T_0\right)^2 k\rho c} \tag{52}$$

respectively, we can write Equation (46) as

$$\tau_{ig} = \frac{\pi}{2\left(2-\beta_{ig}\right)\left(1-\beta_{ig}\right)} \beta_{ig}^2 \tag{53}$$

or by rearranging

$$\frac{1}{\sqrt{\tau_{ig}}} = \left[\frac{2\left(2-\beta_{ig}\right)\left(1-\beta_{ig}\right)}{\pi}\right]^{1/2} \frac{1}{\beta_{ig}} \tag{54}$$

plus the Delichatsios *et al.* high and low heat flux relationships given by Equation (48) and Equation (49) can be written as

$$\frac{1}{\sqrt{\tau_{ig}}} = \frac{2}{\sqrt{\pi}}\left(\frac{1}{\beta_{ig}} - 0.64\right), \qquad \frac{1}{\beta_{ig}} > 3 \tag{55}$$

$$\frac{1}{\sqrt{\tau_{ig}}} = \sqrt{\pi}\left(\frac{1}{\beta_{ig}} - 1\right), \qquad \frac{1}{\beta_{ig}} < 1.1 \tag{56}$$

Figure 4 shows a comparison between the integral model and the Delichatsios *et al.* high and low heat flux equations. The solutions to the two models run parallel at high heat fluxes and both models terminate at the same point at the intercept to the x-axis. The Delichatsios solutions are given for specified limits $\frac{1}{\beta_{ig}}$ (Equation (55) and Equation (56)). By extending the two solutions for the region between the specified limits such that they overlap we find that they cross at around $\frac{1}{\beta_{ig}}$=1.6.

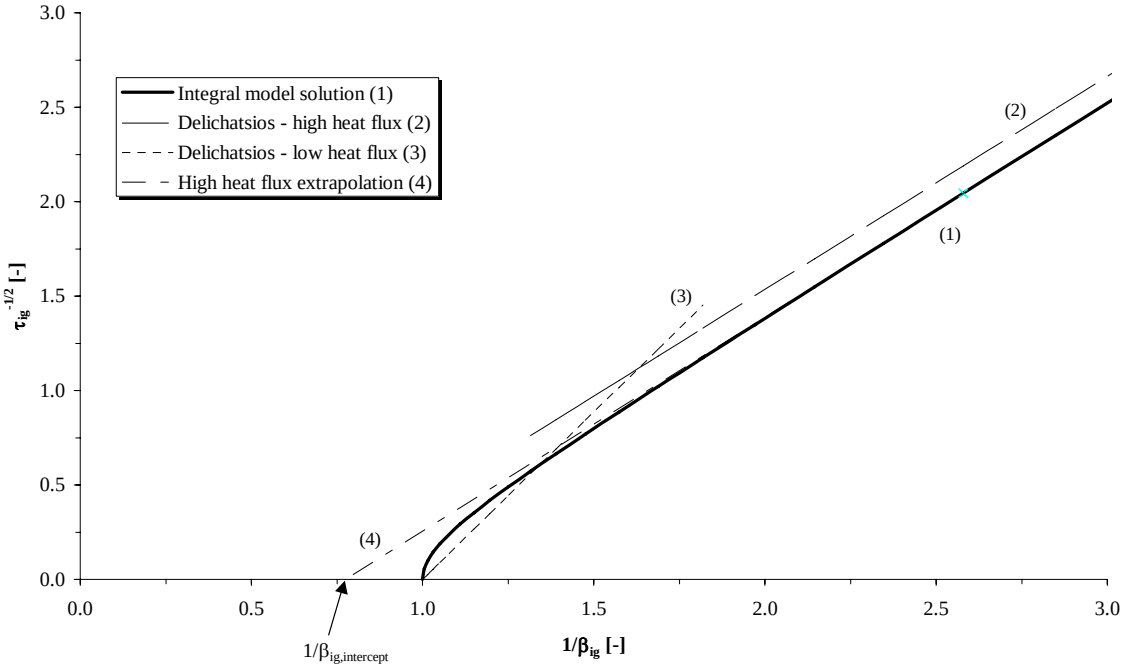

Figure 4. Comparison of the integral model and the Delichatsios *et al.* equations.

Figure 4 also includes the extrapolation of the high heat flux portion of the integral model which shows that there is an error in using such an extrapolation compared with the integral model solution for the determination of the intercept along the x-

axis. Let $\frac{1}{\beta_{ig,intercept}}$ be the intercept of the linear extrapolation of a graph of $\frac{1}{\sqrt{\tau_{ig}}}$ plotted against $\frac{1}{\beta_{ig}}$. From the integral solution given in Equation (54), choosing values of $\frac{1}{\beta_{ig}}$ for two typical high heat flux cases we get

$$\text{when } \frac{1}{\beta_{ig}} = 5, \qquad \frac{1}{\sqrt{\tau_{ig}}} = 4.787$$

$$\text{when } \frac{1}{\beta_{ig}} = 2.5, \qquad \frac{1}{\sqrt{\tau_{ig}}} = 1.954$$

At high heat fluxes, $\beta_{ig} \to 0$ and therefore we can reduce Equation (54) to

$$\frac{1}{\sqrt{\tau_{ig}}} = \frac{2}{\sqrt{\pi}} . \frac{1}{\beta_{ig}} \tag{57}$$

By assuming that the difference between the exact solution and the extrapolated solution is $\left(\frac{1}{\beta_{ig}} - \frac{1}{\beta_{ig,intercept}} \right)$, we can write Equation (54) as

$$\frac{1}{\sqrt{\tau_{ig}}} = \frac{2}{\sqrt{\pi}} . \left(\frac{1}{\beta_{ig}} - \frac{1}{\beta_{ig,intercept}} \right) \tag{58}$$

Substituting in for our approximate values we obtain

$$4.787 = \frac{2}{\sqrt{\pi}} \left(5.0 - \frac{1}{\beta_{ig,intercept}} \right) \qquad \to \qquad \frac{1}{\beta_{ig,intercept}} = 0.758$$

$$1.954 = \frac{2}{\sqrt{\pi}} \left(2.5 - \frac{1}{\beta_{ig,intercept}} \right) \qquad \to \qquad \frac{1}{\beta_{ig,intercept}} = 0.768$$

Hence from Equation (34) the extrapolated intercept is $\frac{\dot{q}_i''}{\dot{q}_{cr}''} \approx 0.76$, thus the critical heat flux is found from

$$\dot{q}_{cr}'' = \frac{\left(\dot{q}_i'' \right)_{intercept}}{0.76} \tag{59}$$

In comparison, from Equation (54) (which is equivalent to Equation (58)), Delichatsios *et al.* obtain a correction factor of 0.64 for the determination of the critical heat flux using high incident flux data. It should be emphasised that this

extrapolation method to the critical heat flux is theoretical and based on a thermal ignition model.

6. ANALYSIS

6.1 Critical heat flux

The critical heat flux can be experimentally obtained by successively exposing samples of the material at decreasing incident heat fluxes until ignition no longer occurs. Thus the critical heat flux is somewhere between the lowest incident heat flux at which ignition occurred and the highest incident heat flux where ignition did not occur. Clearly this approach can be a time consuming process as it may require several tests to find the bounds of critical heat flux depending on the resolution required. In addition, as the critical heat flux is approached, then times to ignition become increasingly longer. Finally, there is the question as to how long one should wait before deciding that ignition will not occur. It was found in this study that ignition may not occur until anything between several tens of minutes and up to one and a half hours have elapsed. Table 2 shows the critical heat fluxes obtained from the ignition experiments where the lowest incident flux at which ignition was obtained is quoted.

Species	Grain orientation	Average moisture content [%]	Measured critical heat flux for ignition [kW/m^2]	Time to ignition [hrs:mins:secs]
Redwood	*along*	8.6	13[1]	0:36:10
	across	7.4	9	0:23:36
Red oak	*along*	5.1	-	-
	across	5.2	-	-
Douglas fir	*along*	7.4	12	1:33:00
	across	8.5	9	0:39:55
Maple	*along*	4.8	12	1:10:00
	across	4.8	8[1]	0:44:40

[1] next lowest integer incident heat flux failed to ignite sample

- no data

Table 2. Critical heat fluxes obtained from experiments.

However, as an alternative to directly obtaining the critical heat flux from an experimental procedure, the critical heat flux can be estimated from time to ignition data by plotting $1/\sqrt{t_{ig}}$ against incident heat flux and then using Equation (59) obtained by the thermal integral model.

In the study of non-charring materials by Hopkins [21], it was suggested that a linear regression through data below 40 kW/m^2 gives a better measure for the critical heat flux since at lower heat fluxes ignition takes longer. This approached seemed to work for non-charring materials but for wood the char oxidation introduces another mechanism for ignition. The simple thermal model based on applied incident heat flux is not sufficient. Examination of $1/\sqrt{t_{ig}}$ against incident heat flux showed that at low heat fluxes the data tends to exhibit a secondary trend towards a very low critical heat flux (Figure 5). This was as a result of the localised glowing ignition discussed in Section 3.3.

Thus, it was decided that the critical heat flux without the effect of the localised heating could be obtained from a linear regression through only the 'high' heat flux measurements and the low heat flux data was not utilised in the determination of the final critical heat flux. In this case, the 'high' heat flux data was taken to be where the incident heat flux was around 20 kW/m^2 or above. The selection of the lower limit of the 'high' heat flux data was based on experimental observations as to at what incident flux the glowing ignition appeared, the shapes of the $1/\sqrt{t_{ig}}$ curves and from the theory. In the case of the theory, Figure 4 suggests that the integral model gives an approximately straight line when $\frac{1}{\beta_{ig}} \geq 1.5$ i.e. $\dot{q}_i'' \geq 1.5\,\dot{q}_{cr}''$. Since values for the experimental critical heat fluxes were found to be at most around 12 kW/m^2 (and 1.5 x 12 = 18) then a 'high' heat flux threshold of 20 kW/m^2 is reasonable. The "1.5" threshold is also comparable to the intersection of around 1.6 for the Delichatsios *et al.* equations.

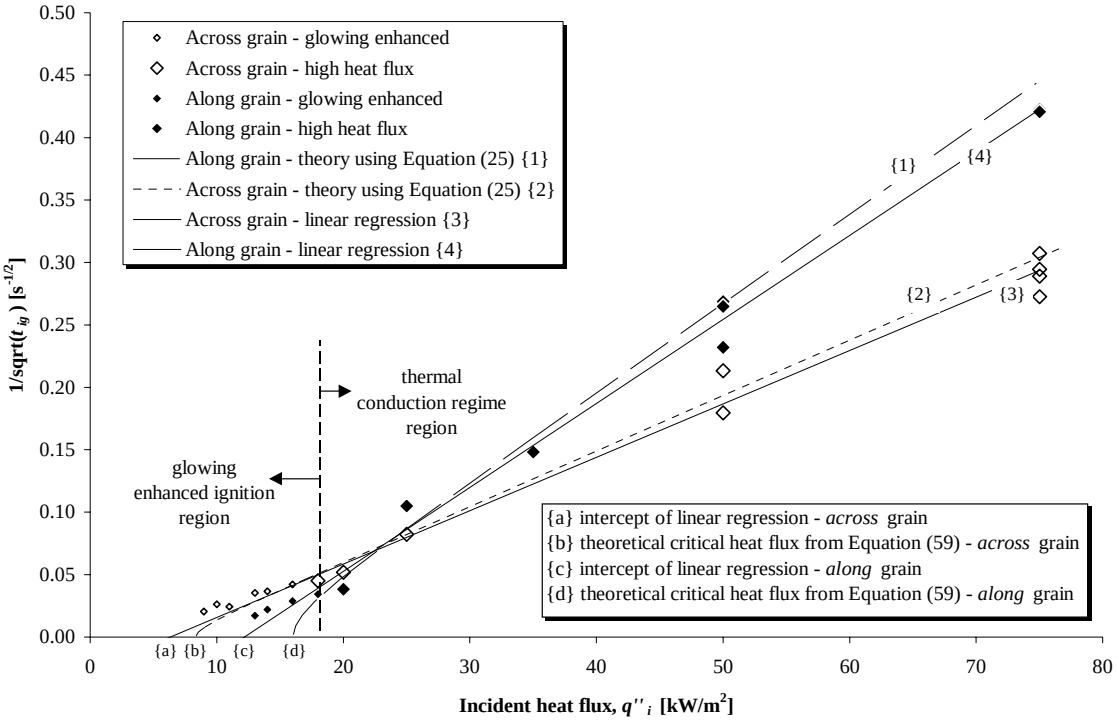

Figure 5. Determination of the critical heat flux for ignition for Douglas fir.

Figure 5 shows the $1/\sqrt{t_{ig}}$ against incident heat flux data for Douglas fir with a linear regression through the 'high' heat flux points shown by large symbols. The figure also shows the intercepts of the linear regression lines and the critical heat fluxes thus obtained from Equation (59). Finally, theoretical curves obtained from Equation (25) using the derived average ignition temperature and thermal inertia (see Section 6.2) are also shown. Table 3 shows the critical heat fluxes obtained from the intercept of the linear regression line for all four species tested.

Species	Grain orientation	Critical heat flux from intercept of $1/\sqrt{t_{ig}}$ against incident heat flux		Final derived critical heat flux using Equation (59) and 'high' flux intercept values (e.g. points {b} and {d} in Figure 5)	Literature values
		'High' flux data (e.g. points {a} and {c} in Figure 5)	All data		
		[kW/m^2]	[kW/m^2]	[kW/m^2]	[kW/m^2]
Redwood	*along*	11.7	11.7	15.5	14.0 [25], 12.4 [26]
	across	4.5	2.6	5.9	-
Red Oak	*along*	8.2	8.2	10.8	10.5 [26]
	across	7.0	7.0	9.2	-
Douglas Fir	*along*	12.2	11.7	16.0	13.0 [25]
	across	6.4	5.7	8.4	-
Maple	*along*	10.6	9.5	13.9	-
	across	2.9	1.1	3.8	-

Table 3. Comparison of critical heat fluxes for ignition using 'high' and all incident heat flux data.

In order to investigate the difference between using only the 'high' heat flux data and all of the data linear regression fits were also made through all of the time to ignition data obtained for the Douglas fir, Redwood and Maple species and the critical heat flux determined. These data are compared with the 'high' heat flux data critical heat flux values in Table 3. In general, the *along* grain orientations show little difference. However, the *across* grain orientations for the Maple and Redwood show significant differences with the 'high' incident flux data giving critical heat fluxes approximately twice are large. There is no difference between the data for the Red oak since no low incident heat flux measurements were made in the experiments. Table 3 also shows the final derived critical heat fluxes for ignition for each specie using the linear regression through the 'high' heat flux data and Equation (59).

The extrapolation process is only an empirical method based on the idea of a smooth continuous function. The method by the thermal integral model ignores any heat flux effect from the glowing so it cannot predict these glowing regime data. The theory using the 'high' flux extrapolated method should give an effective critical flux for the thermal conduction region only.

When the derived and measured critical heat fluxes obtained in this study are compared it can be seen that both methods gave lower critical heat fluxes for the *across* grain orientation. The measured critical heat fluxes for the *along* grain orientation are lower than the derived values whereas the measured *across* grain values are greater than the derived values. These discrepancies between the two sets of data is as a result of the glowing ignition mechanism observed in the experiments that appears to add additional energy to the ignition process which is not included in the theoretical analysis.

An overall comparison of the critical heat flux values derived from the time to ignition data compared with literature values (Table 3) show slightly higher values for the *along* grain orientation and significantly lower values for the *across* grain orientations. The differences in the values may be partly explained by the fact that Tran & White's tests were conducted in the OSU and that Janssens [25] tested his samples in the Cone Calorimeter in the vertical orientation. However, in the study by Atreya *et al.* [12] it was found that the critical heat flux only varied by about 10% between horizontal and vertical samples and the critical heat flux was greater in the vertical case. Thus we might expect Janssens critical heat flux data to be somewhat less if his samples had been tested horizontally.

Moisture content may also have been a factor since the samples tested in this study were not oven dry as were those used by Janssens [25]. As already noted, moisture can increase the time to ignition thus effectively increasing the critical heat flux for ignition. However, Tran & White [26] quoted typical moisture contents of 8-9% for their samples and yet Janssens [25] obtained a critical heat flux for oven dry Redwood which is higher than that given by Tran & White.

Clearly, the determination of the critical heat flux of wood is open to some degree of deviation depending on several factors including the test apparatus and by natural variation in the wood species.

6.2 Average ignition temperature and thermal inertia

By obtaining the critical heat flux for ignition for each species in the *along* and *across* orientations, Equation (33) can be used to solve for the average ignition temperature. Equation (33) was solved numerically by an iterative process for the derived critical heat flux, given by Equation (59) using the 'high' flux data, to obtain a theoretical value for the average ignition temperature.

The apparent thermal inertia can be obtained from the slope of the best-fit line of the plot of $1/\sqrt{t_{ig}}$ against incident heat flux. From Equation (28), at 'high' heat fluxes (as defined in Section 6.1),

$$\dot{q}_i'' = \frac{1}{\sqrt{t_{ig}}}\sqrt{\frac{2}{3}k\rho c}\left(T_{ig} - T_0\right) \tag{60}$$

thus

$$slope = \left[\frac{1}{\sqrt{\frac{2}{3}k\rho c}\left(T_{ig} - T_0\right)}\right] \tag{61}$$

and hence

$$k\rho c = \frac{3}{2}\left[\frac{1}{slope\left(T_{ig} - T_0\right)}\right]^2 \tag{62}$$

Table 4 shows the calculated ignition temperature and apparent thermal inertia obtained for the various species in the *across* and *along* grain configurations.

Species	Grain orientation	Measured average density [kg/m^3]	Theoretical ignition temperature [°C]	Theoretical apparent thermal inertia [kJ^2.m^{-4}K^{-2}s^{-1}]
Redwood	*along*	354	375	0.22
	across	328	204	2.07
Red oak	*along*	753	304	1.01
	across	678	275	1.88
Douglas fir	*along*	502	384	0.25
	across	455	258	1.44
Maple	*along*	741	354	0.67
	across	742	150	10.91

Table 4. Measured and derived properties of wood samples tested.

The thermal degradation characteristics of wood shift towards higher temperatures with the increase in the lignin content of softwoods [23]. This analysis found that the average ignition temperatures for Redwood and Douglas fir (softwoods) are generally greater than those for Red oak and Maple (hardwoods) in the two grain orientations.

The average ignition temperatures obtained in this study were compared with data quoted in the literature. Tran & White [26] measured the ignition temperature of their samples with a thermocouple on the exposed surface of the samples. They quote an average ignition temperature for Redwood as 364 °C. Janssens [25] gives an average ignition temperature from Redwood as 363 °C. Dietenberger [28] gives ignition temperatures of 353 °C in the Cone Calorimeter and values between 290 °C and 356 °C (depending on the moisture content of the samples) in the LIFT [30]. All of these values compare reasonably well with the average temperature calculated in this study for the *along* grain oriented Redwood with the value given here being slightly above those quoted by the other researchers.

Janssens [25] quotes an ignition temperature of 350 °C for Douglas fir which is lower than the temperature of 384 °C calculated in this study for the *along* grain orientation. Tran & White [26] obtained an ignition temperature of 315 °C for Red oak and Atreya

et al. [9] quotes 365 °C. Both of these values are greater than the ignition temperatures obtained in this study for the *along* and *across* grain orientations.

The data from the literature and this study demonstrate that there is a fair degree of variability in the ignition temperatures of wood. As discussed earlier, there are many factors that influence the ignition properties of wood. However, the average ignition temperatures obtained in this study are comparable with the data quoted by other researchers and an average ignition temperature of somewhere between 300 °C and 380 °C for *along* grain oriented wood is typical.

6.3 Ignition temperature and incident heat flux

By rearranging Equation (30) we obtain

$$T_{ig} = T_0 + \sqrt{\frac{t_{ig}\left(\dot{q}_i''\right)^2}{C_{ig} k \rho c}} \tag{63}$$

Using the measured times to ignition and the apparent thermal inertia, the ignition temperature at a given incident heat flux can be calculated with Equation (63). Since C_{ig} also includes T_{ig}, Equation (63) cannot be solved analytically but has to be solved iteratively.

In the study by Hopkins [21], thermocouples were located on the exposed surface of the samples tested so as to obtain the ignition temperatures at given incident heat fluxes. Figure 6 compares these calculated ignition temperatures obtained from Equation (63) for Redwood with those measured by Hopkins [21] and quoted by Tran & White [26] and Janssens [25].

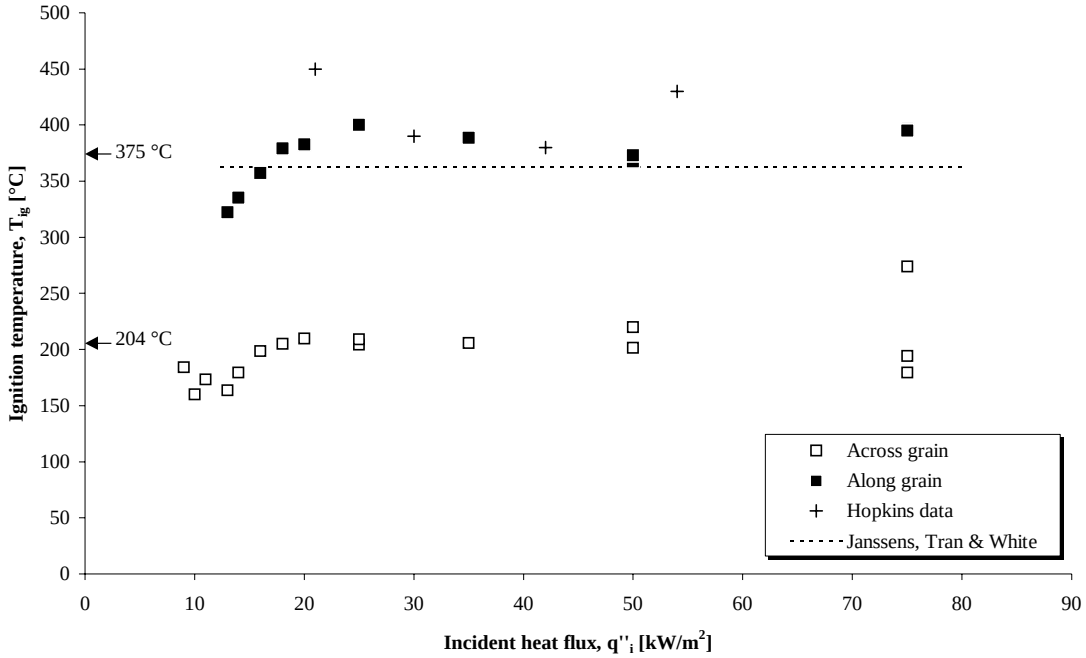

Figure 6. Predicted ignition temperatures for given incident heat fluxes for Redwood.

The calculated ignition temperatures, particularly for the *along* grain configuration, compare well with the other literature data at heat fluxes above around 20 kW/m^2. The ignition temperature quoted by Hopkins at 21 kW/m^2 is greater than those found elsewhere. Below 20 kW/m^2 the calculated ignition temperatures show a downward trend with a limiting value of around 200 °C for the *across* grain configuration. Similar results were obtained for the Douglas Fir and Maple samples in which low heat flux measurements were made.

In all four cases the ignition temperatures are almost constant at incident heat fluxes above around 20 kW/m^2. Simms [6] quotes work by Bamford, Crank & Malan in which it is suggested that at high incident fluxes the energy required for surface ignition appeared to tend to a constant value. The results from this study agree with these findings.

Equation (63) does not include any heat flux contribution by glowing and so it is more appropriate to use it in the thermal conduction regime region. Thus below 20 kW/m^2, it was found that the calculated ignition temperatures using Equation (63) fell to values lower than the constant values found above 20 kW/m^2. However, it is

interesting to note that a similar decrease in the measured ignition temperature of PMMA with decreasing incident heat flux was obtained by Rhodes & Quintiere [40].

The fact that the ignition temperature falls as the incident heat flux is reduced initially appears to conflict with Atreya *et al.* [12] in which they found that the ignition temperature rises as the incident heat flux decreases. However on close examination of their data (for Mahogany) it was found that the minimum incident heat flux used in their experiments was ~18 kW/m^2. The data obtained in this paper for Douglas fir, Redwood and Maple shows that around this same flux region the ignition temperatures also showed a slight rise (such as shown in Figure 6) before decreasing again as the incident flux is further reduced. The ignition temperatures obtained by Hopkins [21] for Redwood also shows a rise at 21 kW/m^2 compared with 30 kW/m^2 and 42 kW/m^2.

6.4 Thermal conductivity and specific heat

Finally, using the derived values for the thermal inertia given in Table 4 and the assumed values for the thermal diffusivity given in Table 1, the thermal conductivity and specific heat at ignition of each species of wood in the two orientations were obtained (Table 5).

Species	Grain orientation	Derived thermal conductivity [W.m^{-1}.K^{-1}]	Derived specific heat [J.kg^{-1}.K^{-1}]
Redwood	*along*	0.19	3,200
	across	0.85	7,400
Red Oak	*along*	0.44	3,100
	across	0.86	3,200
Douglas Fir	*along*	0.23	2,200
	across	0.80	4,000
Maple	*along*	0.35	2,500
	across	2.08	7,100

Table 5. Derived thermal conductivity and specific heat at ignition of the four species of wood tested.

6.5 Dimensionless ignition analysis

The time to ignition against incident heat flux data can be plotted in a dimensionless form. Using Equation (51) and Equation (52), Equation (30) can be written as

$$\frac{1}{\beta_{ig}} = \sqrt{C_{ig}} \frac{1}{\sqrt{\tau_{ig}}} \tag{64}$$

A dimensionless plot of all the ignition data is shown in Figure 7 using the derived critical heat fluxes for each species given in Table 3 to obtain $1/\beta_{ig}$. The plot also shows the theoretical curves with C_{ig} having either the *4/3* or $2\pi/4$ factors. The plot shows that scatter of the data is within the bounds of either the *4/3* or $2\pi/4$ factor used in the theory.

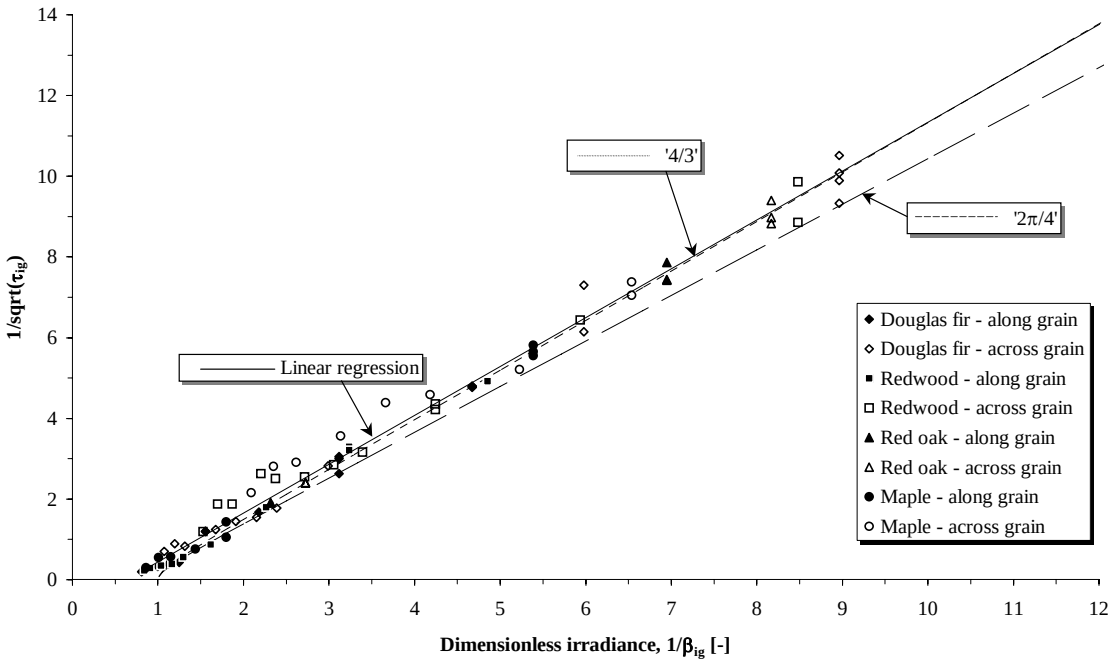

Figure 7. Dimensionless ignition plot on linear scales for all species tested showing comparison between measured ignition times and theoretical values.

The data shown in Figure 7 was plotted on log scales to show the low incident heat flux data more clearly (Figure 8). It can be seen that the experimental data at low heat fluxes does not match the theory. The data does not curve as sharply to $1/\beta_{ig} = 1$ as the integral model solution suggests. This discrepancy between the data and theory is a result of the localised ignition mechanism observed in the experiments as described

in Section 3.3. In the theory we only account for the external heat flux and not any additional energy from the glowing process.

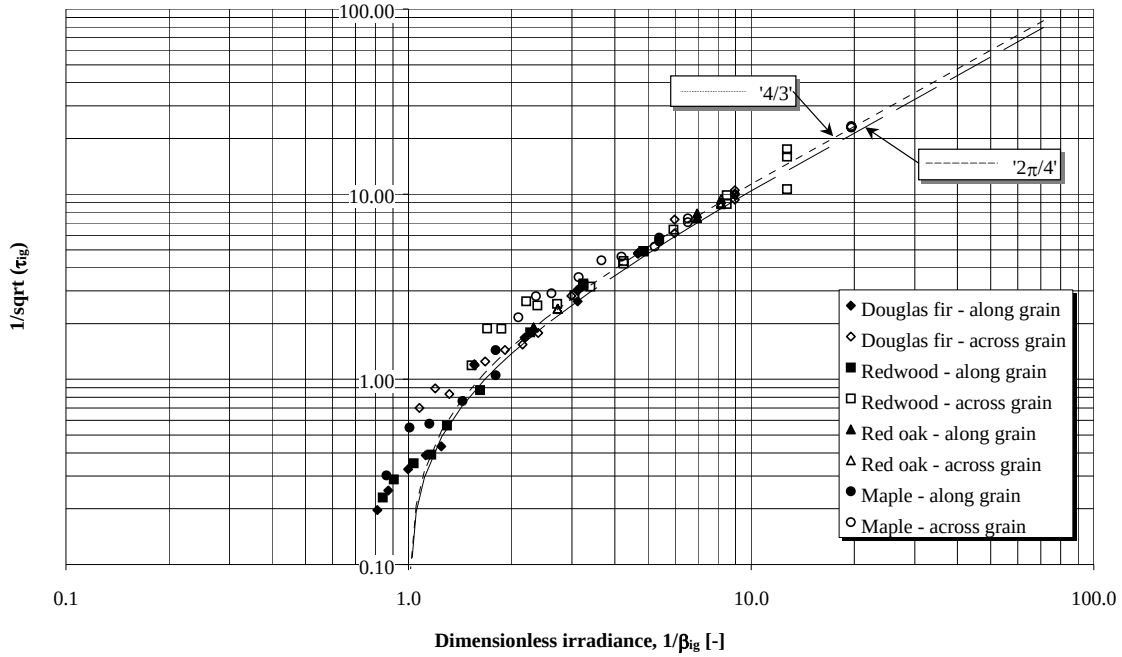

Figure 8. Dimensionless ignition plot on logarithmic scales for all species tested showing comparison between measured ignition times and theoretical values.

From Equation (64) the gradient of the dimensionless plot gives

$$C_{ig} = \left(\frac{1}{gradient} \right)^2 . \tag{65}$$

By plotting a best-fit line through the data shown in Figure 7, a gradient of 1.21 is obtained. Thus, from Equation (65), C_{ig} is found to be 0.68. The value for C_{ig} compares well to the 0.62 quoted by Abu-zaid & Atreya [11] and the gradient of 1.21 is close to the 4/3 predicted by the integral solution.

7. CONCLUSIONS

- The ignition of wood depends on many factors including the species, grain orientation, moisture content, exposure conditions and the inherent variability of wood as a natural material.

- The integral model for the time to ignition gives good agreement with experimental data at high incident heat fluxes (greater than ~20 kW/m^2)
- A low estimate of the critical heat flux for piloted ignition can be obtained from the time to ignition data using the intercept along the x-axis of a linear extrapolation of a plot of $1/\sqrt{t_{ig}}$ against incident heat flux. This intercept value needs to be modified by a constant factor to obtain an estimate of the critical heat flux that is consistent with the integral model.
- An average ignition temperature of wood can be obtained from the critical heat flux derived from the ignition time measurements.
- The apparent thermal inertia of a material can be obtained from the slope of a linear extrapolation of a plot of $1/\sqrt{t_{ig}}$ against incident heat flux and the derived average ignition temperature. Using the apparent thermal inertia and the assumption that the thermal diffusivity remains constant, the thermal conductivity and specific heat of the wood at ignition can be calculated.
- The mechanism for the ignition of wood at low heat fluxes close to the critical heat flux appears to be different from that at high heat fluxes. At low heat fluxes, a small glowing region of the wood may increase the energy input at that point and thus lead to a localised ignition. It is clear that further study of this ignition mechanism is required and that the integral model may have to be modified to account for it.

8. ACKNOWLEDGEMENTS

The authors would like to thank Robert Schroeder for allowing the additional data obtained on behalf of his studies to be used for this analysis and for his provision of extra test samples. The authors also note the partial support given by the Department of Fire Protection Engineering, University of Maryland and NIST/BFRL.

9. REFERENCES

1. Spearpoint M. J. Predicting the ignition and burning rate of wood in the Cone Calorimeter using an integral model. NIST-GCR-99-977, National Institute of Standards and Technology, Gaithersburg, MD, April 1999.
2. Anon. Standard test method for heat and visible smoke release rates for materials and products using an oxygen consumption calorimeter, NFPA 264, 1995. National Fire Protection Association, Quincy, MA.
3. Spearpoint M. J., Quintiere J. G., Predicting the burning of wood using an integral model. Submitted to Combustion & Flame.
4. Kanury A. M., Flaming ignition of solid fuels. SFPE Handbook of Fire Protection Engineering, Second ed., Section 2/Chapter 13, pp.2-190 to 2-204, Society of Fire Protection Engineers, Boston, MA, 1995.
5. Roberts A. F., A review of kinetics data for the pyrolysis of wood and related substances. Combustion and Flame, 14, 261-272 (1970).
6. Simms D. L., Damage to cellulosic solids by thermal radiation. Combustion and Flame, Vol. 6, December 1962 pp.303-318.
7. Kanury A. M., Rate of charring combustion in a fire. Proceedings of the Fourteenth Symposium (International) on Combustion, Pennsylvania State University, 1972.
8. Suuberg E. M., Milosavljevic I., Lilly W. D., Behavior of charring materials in simulated fire environments. NIST-GCR-94-645, National Institute of Standards and Technology, Gaithersburg, MD, 1994.
9. Atreya A., Pyrolysis, ignition and fire spread on horizontal surfaces of wood. PhD thesis, Harvard University, Cambridge, MA, 1983.
10. Tzeng L, Atreya A., Theoretical investigation of piloted ignition of wood. NIST-GCR-91-595, National Institute of Standards and Technology, 1991.
11. Abu-Zaid M., Atreya A. Effect of water on piloted ignition of cellulosic materials. Michigan State Univ., East Lansing National Institute of Standards and Technology, Gaithersburg, MD NIST GCR 89-561; 189 p. February 1989.
12. Atreya A., Carpentier C., Harkleroad M. Effect of sample orientation on piloted ignition and flame spread. Fire Safety Science - Proceedings of the First International Symposium, pp.97-109.
13. Delichatsios M. A., de Ris L., An analytical model for the pyrolysis of charring materials. Factory Mutual Technical Report, 1983.

14. Chen Y., Delichatsios M. A., Motevalli V. Material pyrolysis properties, Part 1: An integral model for one-dimensional transient pyrolysis of charring and non-charring materials. Combustion Science and Technology, Vol. 88 pp.309-328 (1993).
15. Wichman I. S., Atreya A., A simplified model for the pyrolysis of charring materials. Combustion and Flame, Vol. 68, pp.231-247 (1987).
16. Yuen R., Casey R., De Vahl Davis G., Leonardi E., Yeoh G. H., Chandrasekaran V., Grubits S. J. Three dimensional mathematical model for the pyrolysis of wet wood. Fire Safety Science. Proceedings. Fifth International Symposium, Melbourne, Australia, Intl. Assoc. for Fire Safety Science, Boston, MA, Hasemi Y., Editor, 189-200 pp, 1997.
17. Parker W. J., Prediction of the heat release rate of wood, Fire Safety Science - Proceedings of the First International Symposium, pp.207-216.
18. Quintiere J. G., A semi-quantitative model for the burning rate of solid materials. NISTIR 4840, National Institute of Standards and Technology, Gaithersburg, MD, 1992.
19. Quintiere J. G., Iqbal N. Approximate integral model for the burning rate of a thermoplastic-like material. Fire and Materials, Vol. 18, 89-98, 1994.
20. Anderson G. W., A burning rate model for charring materials. NIST-GCR-97-725, National Institute of Standards and Technology, Gaithersburg, MD, 1997.
21. Hopkins D., Predicting the ignition time and burning rate of thermoplastics in the Cone Calorimeter. NIST-GCR-95-677, National Institute of Standards and Technology, Gaithersburg, MD, 1995.
22. Moghtaderi B., Novozhilov V., Fletcher D., Kent J. H., An integral model for the transient pyrolysis of solid materials. Fire and Materials, Vol 21, 7-16 (1997).
23. Janssens M., Fundamental thermophysical characteristics of wood and their role in enclosure fire growth. PhD thesis, 1991.
24. Janssens M., Cone calorimeter measurements of the heat of gasification of wood. Interflam '93, pp549-555.
25. Janssens M., A thermal model for piloted ignition of wood including variable thermophysical properties. Fire Safety Science - Proc. Third International Symposium, pp.167-176.
26. Tran H. C., White R. H., Burning rate of solid wood measured in a heat release calorimeter. Fire and Materials, 16, 197-206 (1992).

27. Parker W. J., Prediction of the heat release rate of Douglas fir, Fire Safety Science - Proceedings of the Second International Symposium, pp.337-346.
28. Dietenberger M. A., Ignitability analysis using the cone calorimeter and LIFT apparatus. Proceedings of the International Conference on Fire Safety, Colombus, Ohio, USA, Product Safety Corporation, 1996, Vol. 22, pp.189-197.
29. Schroeder R., The post fire analysis of construction materials, PhD thesis to be published. University of California, Berkley.
30. Anon. Standard test method for determining material ignition and flame spread properties. ASTM E1321-93. American Society for Testing and Materials, Philadelphia, PA.
31. Martin S. Diffusion-controlled ignition of cellulosic materials by intense radiant energy. Tenth Symposium (International) on Combustion, The Combustion Institute, 1965 pp.877-896.
32. Cholin J. M., Wood and wood-based products. Section 4 Chapter 3. Fire Protection Handbook, 18th Edition, National Fire Protection Association, Quincy, MA, 1997.
33. Fredlund B. A model for heat and mass transfer in timber structures during fire. Institute of Science and Technology, Department of Fire Safety Engineering, Lund University, Sweden, 1988.
34. Forest Products Laboratory, The wood engineering handbook. Second edition. Prentice Hall, New Jersey, 1990.
35. Desch H. E., Dinwoodie J. M., Timber - Structure, properties, conversion and use. Seventh edition. Food Products Press, 1996.
36. Janssens M., Thermo-physical properties for wood pyrolysis models. Fire Technology.
37. Delichatsios M. A., Panagiotou TH., Kiley F., The use of time to ignition data for characterizing the thermal inertia and the minimum (critical) heat flux for ignition or pyrolysis. Combustion and Flame 84 323-332 (1991).
38. Drysdale D., An introduction to fire dynamics. John Wiley & Sons, 1996.
39. Carslaw H. S., Jaeger J. C., Heat conduction in solids. Second Edition, Oxford University Press, London, 1959.
40. Rhodes B. T., Quintiere J. G., Burning rate and flame heat flux for PMMA in a Cone Calorimeter. Fire Safety Journal, 26 (1996) 221-240.